Article

Dynamic Devices. Shape Switching and Substrate Binding in Ion-Controlled Nanomechanical Molecular Tweezers

Anne Petitjean, Richard G. Khoury, Nathalie Kyritsakas, and Jean-Marie Lehn

J. Am. Chem. Soc., **2004**, 126 (21), 6637-6647• DOI: 10.1021/ja031915r • Publication Date (Web): 05 May 2004

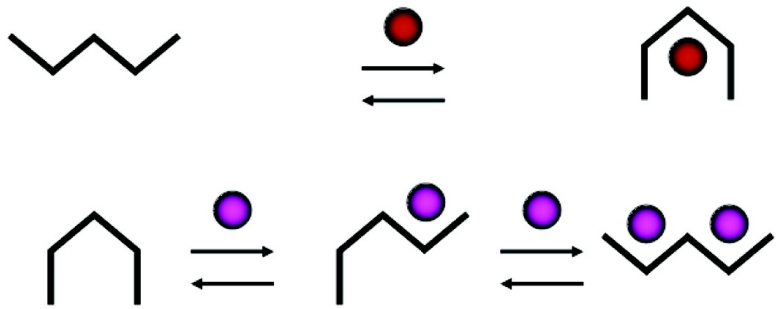

J|A|C|S
ARTICLES
Published on Web 05/05/2004

Dynamic Devices. Shape Switching and Substrate Binding in Ion-Controlled Nanomechanical Molecular Tweezers

Anne Petitjean,[†,§] Richard G. Khoury,[†] Nathalie Kyritsakas,[‡] and Jean-Marie Lehn*[,†]

Contribution from the Laboratoire de Chimie Supramoléculaire, Institut de Science et d'Ingénierie Supramoléculaires, Université Louis Pasteur, 8 Allée Gaspard Monge, BP 70028, 67083 Strasbourg Cedex, France, and Service Commun de Rayons X., Institut Le Bel, Université Louis Pasteur, 4, rue Blaise Pascal, F-6700 Strasbourg, France

Received December 23, 2003; E-mail: lehn@isis.u-strasbg.fr

Abstract: As examples of supramolecular devices performing chemical (ionic, molecular) control of binding events and models of related natural systems, two molecular conformational switches are described, which display cation-controlled nanomechanical motion coupled to substrate binding and release. The substrate binding relies on donor/acceptor interactions, provided by intercalation between planar sites located at the extremities of the switching units, whereas cation complexation is responsible for conformational regulation. The terpyridine **py-py-py**-based receptor is activated toward substrate binding upon complexation of a zinc(II) cation and operates in a two-state process. The replacement of the central pyridine by a 4,6-disubstituted pyridimine as in **py-pym-py** induces a state reversal and yields a new receptor which binds a substrate in the absence of cation, and releases it when copper(I) is introduced, following a three-step process. These systems represent effector-triggered supramolecular switching devices leading toward multistate nanomechanical chemical systems. These two systems illustrate the use of simple conformational switches in the binding site and allosteric regulation of substrate affinity.

Introduction

The controlled triggering of molecular shape changes is of interest both for its relationship to diverse biological processes and for its significance as an elementary component in motional dynamic devices. Living organisms make extensive use of supramolecular systems that are able to convert photochemical or electrochemical processes into (electro)chemical and mechanical energies, essential in building up energy reservoirs, in inducing movement, and in signaling. This energy conversion or relay often results from a change of shape, at the heart of which lies a molecular unit that is able to switch between two or more states of different geometry. For instance, the photoisomerizable pigment retinal participates in the conversion of light into processes as varied as building up cation (H^+ in bacteriorhodopsin)[1] and anion (Cl^- in halorhodopsin)[2] gradients, and neuronal signaling (vision).[3]

In addition to light, ion concentration and gradients are also used to modulate reactivity (e.g., H^+ and Ca^{2+} ATPases, Ca^{2+}-dependent phosphatases and kinases), movement (e.g., Ca^{2+} binding troponin in muscle contraction), and substrate affinity (e.g., Ca^{2+}-dependent binding of recoverin to G-protein in vision), as a result of conformational changes.[4] The latter substrate binding regulation controlled by conformational switching is the basis of the mode of action of G-protein coupled receptors, ubiquitous proteins that bind and activate G-proteins, and ultimately of cell hyperpolarization, upon light or ligand (hormones, neurotransmitters) induction.[3,5]

On the other hand, biological molecules may serve in the derivation of artificial systems undergoing molecular motions, as has in particular been done using DNA as the framework.[6]

Chemistry allows nanomechanical devices[7,8] to be set up without having to resort to molecules of biological type, offering greater diversity, better structural and dynamic control, as well as more compact size. Thus, stimuli-responsive systems undergoing photo- and electrochemically induced motions are well-

[†] Laboratoire de Chimie Supramoléculaire.
[‡] Service Commun de Rayons X.
[§] Present address: Division of Chemistry and Chemical Engineering, California Institute of Technology, 1200 E. California Boulevard, Pasadena, CA 91125.

(1) Neutze, R.; Pebay-Peyroula, E.; Edman, K.; Royant, A.; Navarro, J.; Landau, E. M. *Biochim. Biophys. Acta* **2002**, *1565*, 144−167.
(2) Kolbe, M.; Besir, H.; Essen, L.-O.; Oesterhelt, D. *Science* **2000**, *288*, 1390−1396.
(3) Stenkamp, R. E.; Teller, D. C.; Palczewski, K. *ChemBioChem* **2002**, *3*, 963−967.
(4) (a) Fráusto da Silva, J. J. R.; Williams, R. J. P. *The Biological Chemistry of the Elements, the Inorganic Chemistry of Life*; Oxford University Press: Oxford, 1991; Chapter 10. (b) Concha, N. O.; Head, J. F.; Kaetzel, M. A.; Dedman, J. R.; Seaton, B. A. *Science* **1993**, *261*, 1321−1324. (c) Bajorath, J.; Raghunathan, S.; Hinrichs, W.; Saenger, W. *Nature* **1989**, *337*, 481−484.
(5) Hamm, H. E. *Proc. Natl. Acad. Sci. U.S.A.* **2001**, *98*, 4819−4821.
(6) (a) Niemeyer, C. M.; Adler, M. *Angew. Chem., Int. Ed.* **2002**, *41*, 3779−3783. (b) Mao, C.; Sun, W.; Shen, Z.; Seeman, N. C. *Nature* **1999**, *397*, 144−146.
(7) (a) Lehn, J.-M. *Supramolecular Chemistry Concepts and Perspectives*; VCH: Weinheim, 1995. (b) Lehn, J.-M. In *Supramolecular Science: Where It Is and Where It Is Going*; Ungaro, R., Dalcanale, E., Eds.; Kluwer: Dordrecht, The Netherlands, 1999; pp 287−304.
(8) (a) Balzani, V.; Credi, A.; Raymo, M.; Stoddart, J. F. *Angew. Chem., Int. Ed.* **2000**, *39*, 3348−3391. (b) Stoddart, J. F., Ed. *Acc. Chem. Res.* **2001**, *34*, 409−522. (c) *Molecular Switches*; Feringa, B., Ed.; Wiley-VCH: Weinheim, 2001. (d) For an early example, see: Shinkai, S.; Nakaji, T.; Ogawa, T.; Shigematsu, K.; Manabe, O. *J. Am. Chem. Soc.* **1981**, *103*, 111−115.

10.1021/ja031915r CCC: $27.50

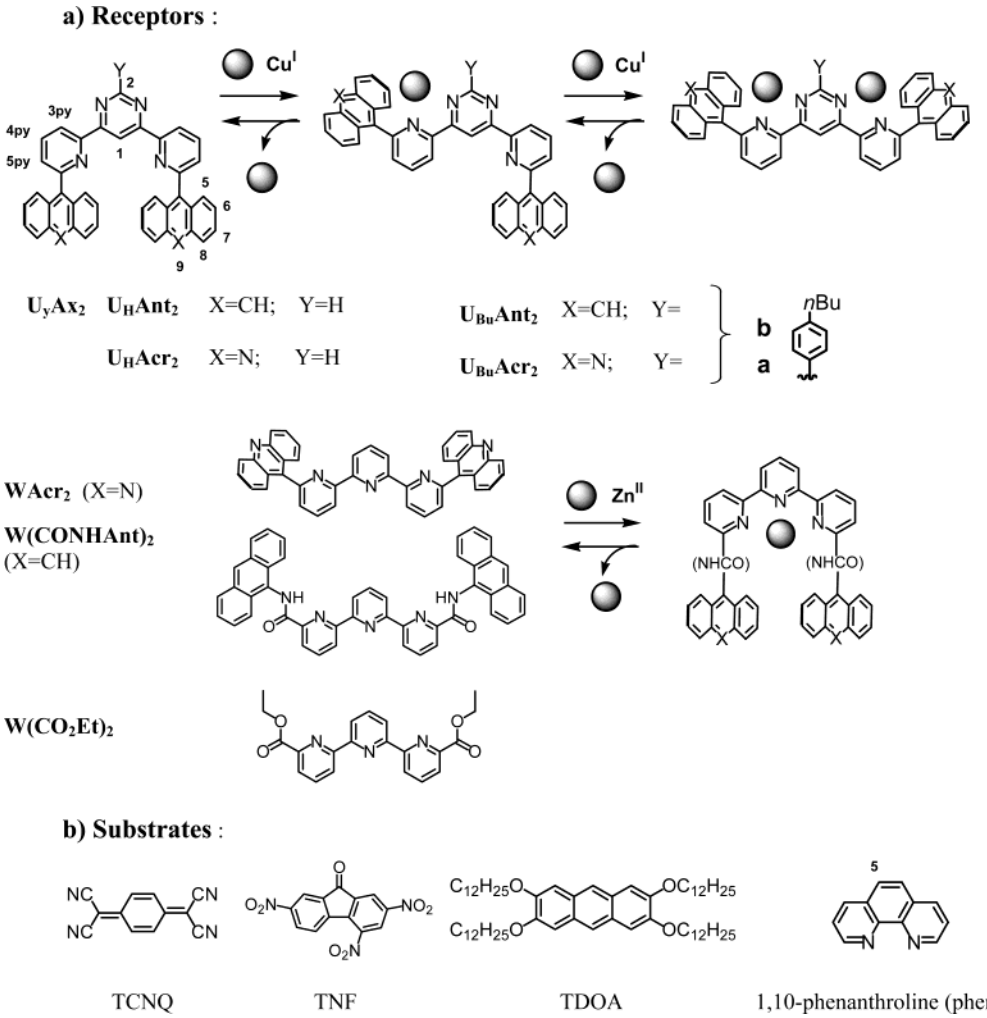

Figure 1. (a) Structures of the receptors and representation of the structural changes resulting from switching processes induced by ion binding. (b) Substrates studied herein.

documented, from the classical cis−trans isomerization of azobenzene derivatives to linear and circular displacements in rotaxanes and catenanes.[8]

Nanomechanical motions may also be induced by ion binding or protonation as is the case for molecular strands undergoing large amplitude extension/contraction motions.[9,10] They may involve shape switching between two (or more) forms presenting different physicochemical properties such as optical effects or substrate binding and release. The latter is of particular interest because it involves the modulation of a recognition/binding process by an external stimulus that induces a motional/mechanical shape switching. It has received attention for instance in the domain of sugar and carboxylic acid recognition.[11]

Concept: Design of Two Complementary Ion-Triggered Shape Switching Systems. As dynamic devices undergoing ion-induced conformational changes that modulate substrate affinity, we report here two types of disubstituted heterocyclic triads designed to switch between U and W shapes upon cation coordination and, as a consequence, that bind by intercalation or release a substrate much like hand-controlled mechanical tweezers. Electron donor and acceptor groups were appended to these triads as substrate binding sites, allowing the presence of bound substrate to be easily monitored via the formation of (colored) charge-transfer complexes.

The two triads studied were designed to have complementary behaviors. The pyridine-pyrimidine-pyridine sequence (**py-pym-py**, $\mathbf{U_yAx_2}$, Figure 1) was anticipated to adopt a U-shaped conformation, placing the two substituents in the 6,6″ position of the pyridine units in parallel planes, at a 7 Å distance well adapted for donor/acceptor $\pi-\pi$ interactions. The self-organization into a U-shaped molecule stems from the preferential transoid conformation of 2,2′-bipyridine (bipy)[12] and related heterobiaryls, which is also the basis of the controlled helical folding of extended polyheterocyclic strands.[13] Just as bipy is converted from a transoid to a cisoid form via metal coordina-

(9) (a) Barboiu, M.; Lehn, J.-M. *Proc. Natl. Acad. Sci. U.S.A.* **2002**, 5201−5206. (b) Barboiu, M.; Vaughan, G.; Kyritsakas, N.; Lehn, J.-M. *Chem.-Eur. J.* **2003**, *9*, 763−769.
(10) (a) Dolain, C.; Maurizot, V.; Huc, I. *Angew. Chem., Int. Ed.* **2003**, *42*, 2738−2740. (b) Kolomiets, E.; Berl, V.; Odriozola, I.; Stadler, A.-M.; Kyritsakas, N.; Lehn, J.-M. *Chem. Commun.* **2003**, 2868−2869.
(11) Shinkai, S. In *Molecular Switches*; Feringa, B., Ed.; Wiley-VCH: Weinheim, 2001; pp 281−307.
(12) Howard, S. T. *J. Am. Chem. Soc.* **1996**, *118*, 10269−10274.
(13) (a) Hanan, G.; Lehn, J.-M.; Kyritsakas, N.; Fischer, J. *J. Chem. Soc., Chem. Commun.* **1995**, 757−766. (b) Ohkita, M.; Lehn, J.-M.; Baum, G.; Fenske, D. *Chem.-Eur. J.* **1999**, *5*, 3471−3481. (c) Cuccia, L. A.; Lehn, J.-M.; Homo, J.-C.; Schmutz, M. *Angew. Chem.* **2000**, *112*, 239−243. (d) Cuccia, L. A.; Ruiz, E.; Lehn, J.-M.; Homo, J.-C.; Schmutz, M. *Chem.-Eur. J.* **2002**, *8*, 3448−3457. (e) Petitjean, A.; Cuccia, L. A.; Lehn, J.-M.; Nierengarten, H.; Schmutz, M. *Angew. Chem., Int. Ed.* **2002**, *41*, 1195−1198.

Scheme 1. Schematic Representation of the Two-Stage U/W (Top) and Three-Stage W/S/U (Bottom) Molecular Shape Switching Processes Induced by Binding of Metal Ions to a **Py-py-py** Sequence and a **Py-pym-py** Sequence, Respectively[a]

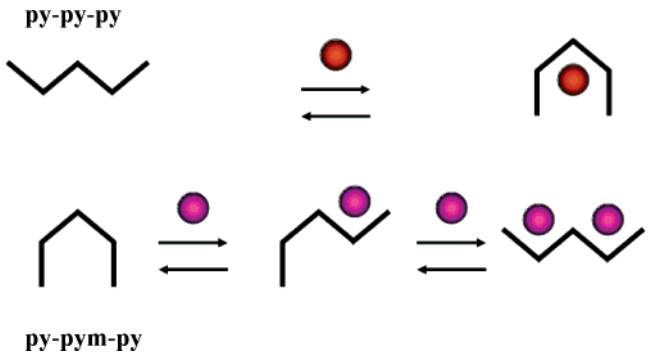

[a] Note the reversal of the shapes of the metal ion free and the ion bound entities upon exchange of the central pyrimidine unit of **py-pym-py** for a pyridine unit in **py-py-py**.

tion, we expected that introduction of N-coordinating cations would switch $\mathbf{U_yAx_2}$ from a U to a W shape, presenting a geometry unsuited for the intercalative binding of a planar substrate. The **py-pym-py** triad should therefore behave like molecular tweezers, releasing the guest upon cation complexation. Conversely, the replacement of the **pym** unit by a **py** group leads to a state reversal, so that the [2,2′;6′,2″]terpyridine (terpy) **py-py-py**-derived coumpounds $\mathbf{WAcr_2}$ and $\mathbf{W(CONHAnt)_2}$ (Figure 1), in which the terminal pyridines are substituted in the 6 and 6″ positions, can be expected to switch, upon coordination of a metal cation, from a noncomplexing uncoordinated W shape to a U conformation suitable for intercalative binding of a substrate species. These U/W shape switching processes upon cation binding are also schematically represented in Scheme 1.

Structural switching upon metal ion coordination has been described recently for β-sheet folding of bipyridine-derived peptides,[14] for tuning of electronic coupling in a bishydroquinone-terpy,[15] and for lanthanide complexes displaying intercalative binding to DNA.[16] A related bispyrenyl-terpy shows coupled optical/structural switching.[17] U-shaped blocked ligands have been shown to bind planar substrate species by intercalation,[18a] and tweezer-type binding by molecular clefts and clips has been subject to recent studies.[18b−g]

Results and Discussion

Ion-Induced Substrate Release: The py-pym-py Sequence. Structure and Conformation of the Free Receptors. As anticipated, the conformational information encoded in bipy-type units leads to the preorganization of the **py-pym-py** sequence into a U-shaped receptor, confirmed in the solid state by the X-ray structures of $\mathbf{U_HAcr_2}$, $\mathbf{U_{Bu}Acr_2H_2}^{2+}$, and $\mathbf{U_HAcr_2Me}^{+}$ (Figure 2, **a**, **b**, and **c**, respectively). In all of these cases, the nitrogen atoms of consecutive ortho-connected bisheteroaryl units adopt the strongly favored (by about 25−30 kJ mol^{-1})[12] transoid orientation (Figure 2, $\mathbf{a_1}$, $\mathbf{b_1}$, and $\mathbf{c_1}$). The propensity of these receptors to accommodate aromatic guests is illustrated in the structure of the receptors alone, because they all form self-complexes in the solid state (Figure 2, $\mathbf{a_2}$, $\mathbf{b_2}$, and $\mathbf{c_2}$; for self-complexes of molecular clips, see for instance ref 18g). The rotation around the connections allows for conformational flexibility, generating a twisted shape in $\mathbf{U_HAcr_2}$ (Figure 2, $\mathbf{a_2}$), whereas aligned aromatic planes, promoted by a planar all-trans **py-pym-py** scaffold, are well adapted for cation−π interactions within the cationic species $\mathbf{U_{Bu}Acr_2H_2}^{2+}$ and $\mathbf{U_HAcr_2Me}^{+}$ (Figure 2, $\mathbf{b_2}$ and $\mathbf{c_2}$). No sign of self-association of these receptors was observed in millimolar solutions with the solvents used in the present studies, as evidenced by the concentration-independent ^{1}H NMR chemical shifts of the receptors. The pyridine H_3 and pyrimidine H_5 protons (numbered 3py and 1, respectively, in Figure 1) show markedly high chemical shifts in solution (1.2−1.5 ppm higher than in the spectra of the corresponding nonsubstituted heterocycles), whereas the protons belonging to the aromatic 6 and 6″ substituents are slightly shielded (−0.1 to −0.3 ppm), consistent with an overall U-shape in solution as well (even in the protonated or methylated species where two positive charges face each other).

Donor/Acceptor Substrate Binding by the U-Shaped Neutral Receptors. Formation and Structure of the Supramolecular Adducts. The introduction of electron acceptors (TNF, TCNQ) into a solution of bis-donors such as $\mathbf{U_yAcr_2}$ and $\mathbf{U_yAnt_2}$ (y = H and Bu) causes the immediate coloration of the solution (red and green, respectively), suggestive of charge-transfer complexation. To analyze the structure of the adducts, ^{1}H NMR studies were conducted in solution. Figure 3 shows the evolution of the chemical shifts of the protons of the receptor and guest (marked by a star) as a concentrated solution of the electron-poor TNF substrate was titrated into a solution of the electron-rich $\mathbf{U_HAnt_2}$ in $CDCl_3$. The complexation of guests by this type of receptors is a fast process on the NMR time scale. The signals of the external protons (on the pyridines and pyrimidine H_2) are not particularly affected, contrary to those of the protons located in the U-cavity; the signal of the pyrimidine proton H1 moves to higher chemical shift, whereas the anthracene protons (H8 and H9 in particular) are significantly shielded. These effects provide evidence for the conservation of the conformation of the receptor within the complex and for the intercalation of the guest between the two aromatic donors. The signals of the TNF protons are also globally shielded (best seen at the beginning of the titration, when most of the guest is complexed). An orientation in which the carbonyl of the TNF points toward the inside of the cavity would explain the strong effect on receptor proton H1. This hypothesis was confirmed by the crystal structure of the red complex [TNF ⊂ $\mathbf{U_HAnt_2}$], represented in Figure 4. The TNF substrate is in van der Waals contact with the two anthracene donors held 7 Å apart and almost parallel (slight pinching) by the U-shaped **py-pym-py**

(14) Schneider, J. P.; Kelly, J. W. *J. Am. Chem. Soc.* **1995**, *117*, 2533−2546.
(15) Büschel, M.; Helldobler, M.; Daub, J. *Chem. Commun.* **2002**, 1338−1339.
(16) Glover, P. B.; Ashton, P. R.; Childs, L. J.; Rodger, A.; Kercher, M.; Williams, R. M.; De Cola, L.; Pikramenou, Z. *J. Am. Chem. Soc.* **2003**, *125*, 9918−9919.
(17) Barboiu, M.; Lehn, J. M., unpublished work.
(18) (a) Sommer, R. D.; Rheingold, A. L.; Goshe, A. J.; Bosnich, B. *J. Am. Chem. Soc.* **2001**, *123*, 3940−3952. Crowley, J. D.; Goshe, A. J.; Bosnich, B. *Chem. Commun.* **2003**, 392−393. Goshe, A. J.; Steele, I. M.; Ceccarelli, C.; Rheingold, A. L.; Bosnich, B. *Proc. Natl. Acad. Sci. U.S.A.* **2003**, *99*, 4823−4829. (b) Molt, O.; Rübeling, D.; Schrader, T. *J. Am. Chem. Soc.* **2003**, *125*, 12086−12087. (c) Proni, G.; Pesticelli, G.; Huang, X.; Nakanishi, K.; Berova, N. *J. Am. Chem. Soc.* **2003**, *125*, 12914−12927. (d) Colquhoun, H. M.; Zhu, Z.; Williams, D. J. *Org. Lett.* **2003**, *5*, 4353−4356. (e) Sijbesma, R. P.; Nolte, R. J. M. *Top. Curr. Chem.* **1995**, *175*, 25−56. (f) Klärner, F.-G.; Kahlert, B. *Acc. Chem. Res.* **2003**, *36*, 919−932. (g) Wu, A.; Chakraborty, A.; Fettinger, J. C.; Flowers, R. A., II; Isaacs, L. *Angew. Chem., Int. Ed.* **2002**, *41*, 4028−4031. (h) Zimmerman, S. C. *Top. Curr. Chem.* **1993**, *165*, 71−102.

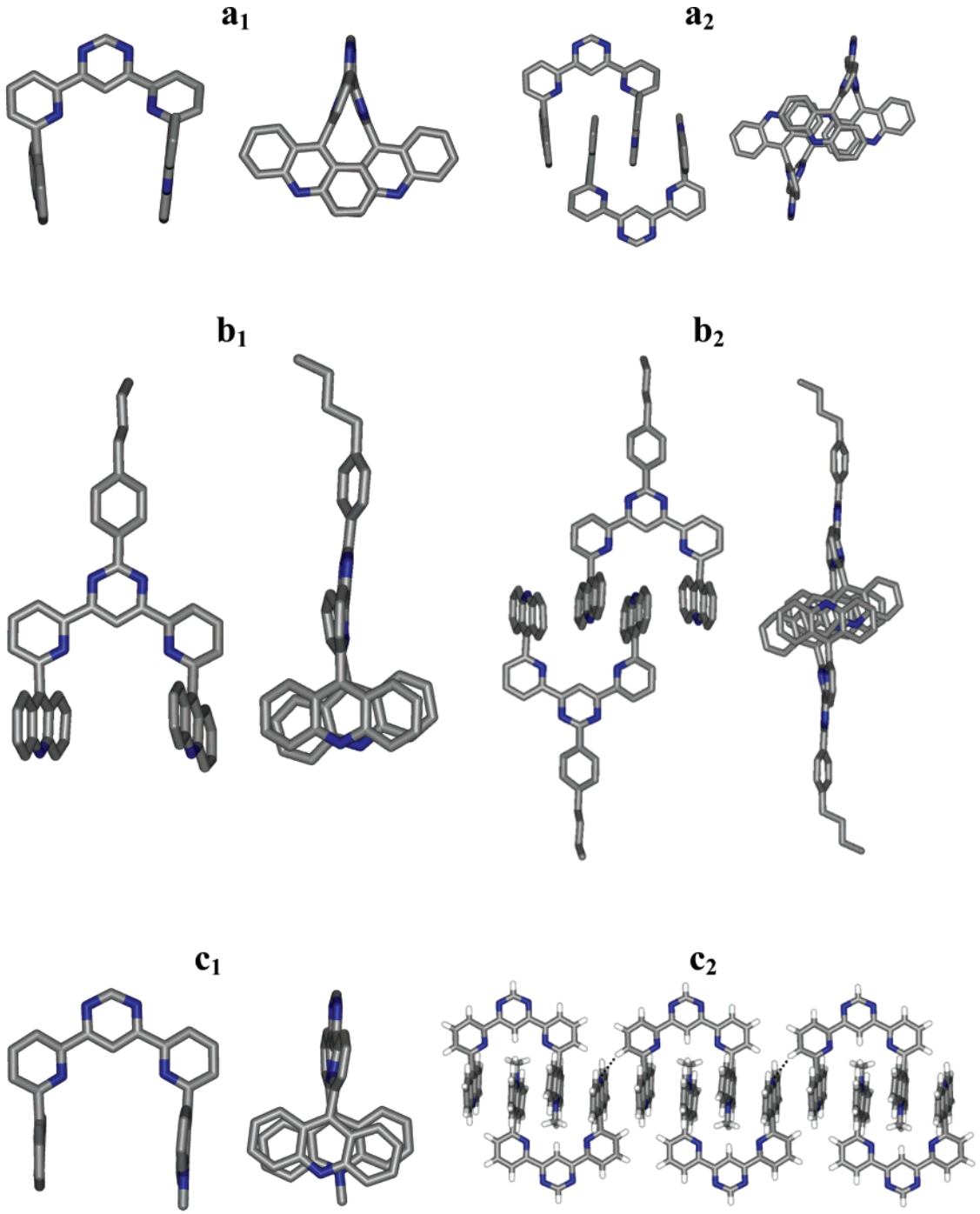

Figure 2. Crystal structures of the receptors (a) $\mathbf{U_HAcr_2}$, (b) $\mathbf{U_{Bu}Acr_2H_2}\cdot 2CF_3CO_2$, and (c) $\mathbf{U_HAcr_2Me}\cdot CF_3SO_3$; solvent molecules and anions are omitted for clarity. $\mathbf{a_1}$, $\mathbf{b_1}$, and $\mathbf{c_1}$: face and side views of a single receptor. $\mathbf{a_2}$, $\mathbf{b_2}$, and $\mathbf{c_2}$: interactions between molecules in the solid state.

sequence, with its carbonyl group located close to the pyrimidine proton H1 and its framework covered by the π cloud of the receptor. The binding affinity of TNF for the receptor was evaluated on the basis of the ^{1}H NMR data and is reported in Table 1, together with the binding constants, determined in similar fashion from ^{1}H NMR titration data, for all of the receptors studied with two electron acceptors (TNF, TCNQ) and an electron donor (TDOA).

U to W Shape Conformational Switching. The conformational behavior of the receptor alone was monitored by ^{1}H NMR titration (data not shown) of a solution of $\mathbf{U_{Bu}Ant_2}$ with $Cu(CH_3CN)_4$, BF_4 in a 1.0:1.0 $CDCl_3/CD_3CN$ mixture. Upon copper(I) addition, the signals corresponding to the anthracene moiety move to higher chemical shifts, consistent with the loss of the shielding mutually exerted by the two anthracene moieties, and the pyridine 3py proton moves to lower chemical shift, consistent with a transoid to cisoid conformational change of the heterocyclic scaffold. More significant is the shielding of the aromatic protons borne by the pyrimidine substituent (located on carbon 2; protons Ha and Hb, Figure 1; the effect is also noticeable in Figure 5), which results from the rotation of the phenyl moiety by ~90° (perpendicular to the plane of the **pym** group) due to the incorporation of the cation coordination sphere in the vicinity and of the shielding caused by the anthracene

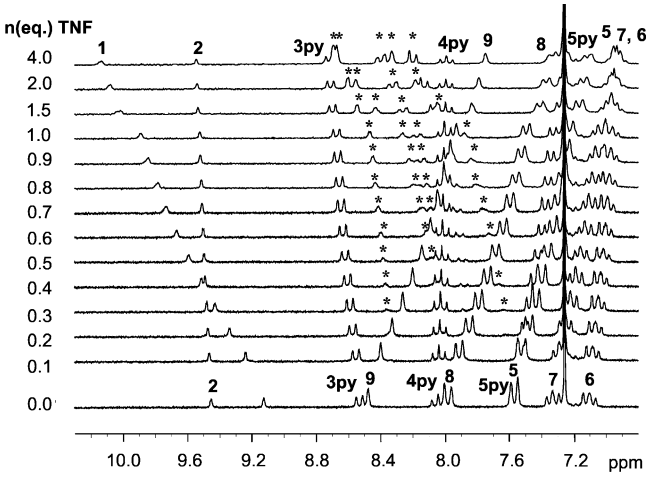

Figure 3. 200 MHz ^{1}H NMR spectral modifications on titration of TNF (8.8 mM solution in $CDCl_3$) into a 3.5 mM solution of $\mathbf{U_HAnt_2}$ ($CDCl_3$; spectrum of the receptor alone at the bottom). The signals of the TNF substrate are marked with a star, and numbering is displayed in Figure 1.

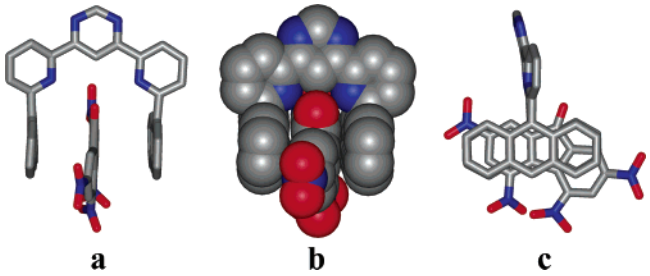

Figure 4. Crystal structure of the complex [TNF ⊂ $\mathbf{U_HAnt_2}$]: (a) ball-and-stick and (b) CPK representation of the face view; (c) side view of the complex, showing the stacking patterns (due to guest disorder in the crystal, the TNF guest appears to bear four nitro groups instead of the actual three).

Table 1. Binding Constants Obtained from ^{1}H NMR Spectral Data[a]

receptor	substrate	$\log_{10}(K_{assoc})$ (K_{assoc}), solvent, 298 K
$\mathbf{U_HAnt_2}$	TCNQ	3.79 ± 0.05 (6200 ± 700 M^{-1}), $CDCl_3$
$\mathbf{U_HAnt_2}$	TNF	3.40 ± 0.06 (2500 ± 500 M^{-1}), $CDCl_3$
$\mathbf{U_HAcr_2}$	TCNQ	2.0 ± 0.1 (~100 M^{-1}), $CDCl_3$
$\mathbf{U_{Bu}Acr_2}$	TNF	1.7 ± 0.2 (~50 M^{-1}), $CDCl_3$
$\mathbf{U_{Bu}Acr_2Me_2}^{2+}$	TDOA	3.00 ± 0.05 (1020 ± 60 M^{-1}), $CDCl_3$ (8% CD_3OD)
[Zn^{II} ⊂ $\mathbf{W(CONHAnt)_2}$]	TNF	1.96 ± 0.4 (130 ± 90 M^{-1}), CD_3CN
[Zn^{II} ⊂ $\mathbf{W(CONHAnt)_2}$]	TCNQ	1.91 ± 0.12 (85 ± 20 M^{-1}), CD_3CN

[a] Obtained by fitting the ^{1}H NMR titration data using the Chem. Equili. Software (version 6.1, 1998, V. P. Solov'ev, Moscow University).

substituents in a W conformation. The conformational switching from U to W shape was confirmed by the observation of ROESY cross-peak between H1 and H3py (data not shown).

Substrate Release Induced by Cation Coordination. Figure 5 shows the evolution of the chemical shifts of the protons of the substrate and of the receptor as cuprous ions are added to a solution of $\mathbf{U_{Bu}Ant_2}$ in 2.0:1.0 $CDCl_3/CD_3CN$ (right scale), containing only 0.5 equiv of TNF substrate so as to ensure that the chemical shifts observed for the guest (average between the complexed and free species) are close enough to the values of the fully complexed state (first three spectra at the bottom of Figure 5; the signals corresponding to the guest are indicated in red). As the addition of a concentrated solution of $Cu(CH_3CN)_4$, BF_4 in the same mixture of solvents (left scale) proceeds, the signals of TNF are gradually deshielded and eventually stabilize at the same value as for TNF alone in the same solvent mixture (top spectrum), indicative of complete release of the guest in solution. The signals of the receptor are also in accordance with the conversion to the W shape (note the strong shielding of protons Hb), where no interaction with the guest can be detected by NMR or visually, as the color of the solution changes from red to brown-yellow, the color of the copper(I) complex of $\mathbf{U_{Bu}Ant_2}$. A similar experiment with a stronger acceptor substrate such as TCNQ gives rise to the same behavior, with the loss of the green color of the charge-transfer TCNQ inclusion complex.

Ion-Induced Guest Binding: The py-py-py Sequence. Structure and Conformation of the Free Receptors $\mathbf{WAcr_2}$ and $\mathbf{W(CONHAnt)_2}$. The known transoid conformational preference of bipy holds for the terpy group, as has been confirmed by X-ray crystallography.[19] The chemical shifts of the signals of the 3, 3′, 5′, and 3″ protons of the parent $\mathbf{W(CO_2Et)_2}$ compound are 1−1.5 ppm downfield as compared to ethyl 2-pyridinecarboxylate and pyridine, consistent with the vicinity of the nitrogen atom of the neighboring ring, and the anthracene and acridine moieties in $\mathbf{WAcr_2}$ and $\mathbf{W(CONHAnt)_2}$ do not experience ring current shielding. Both effects agree with a W conformation.

U to W Shape Conformational Switching. The conformational behavior of the terpy motif was monitored by ^{1}H NMR titration (data not shown) of a solution of $\mathbf{W(CO_2Et)_2}$ in a 1.7:1.0 mixture of $CDCl_3$ and CD_3CN with a concentrated solution of zinc triflate in the same solvent and showed that the initial species was converted into a single new species in a slow process, completed once 1.0 equiv had been added. In the case of this receptor, no trace of the bisterpyridine zinc complex was detected, the carbonyl oxygen of the ester groups probably taking part in the coordination sphere around the cation. During this process, the signals of the protons H3 of the external pyridines move to lower chemical shifts.

Cation-Induced Substrate Binding to the Receptors $\mathbf{WAcr_2}$ and $\mathbf{W(CONHAnt)_2}$. Formation and Structure of the Supramolecular Adducts. The ability of the terpyridine motif to perform guest binding upon coordination was first studied using a coordinating guest. One equivalent of 1,10-phenanthroline (phen) was mixed with $\mathbf{WAcr_2}$ in a 1.7:1.0 mixture of $CDCl_3$ and CD_3CN, and a concentrated solution of zinc triflate in the same solvent was gradually added. If the ^{1}H NMR signals of the phen guest and receptor show no sign of interaction (data not shown) in the absence of zinc, the phen signals indicate that it first binds to the cation (maximal complexation after 0.4 equiv of zinc triflate, slow exchange). After 0.4 equiv is added, this first complex disappears and a mixed complex appears involving the protons of the receptor and of the guest (slow exchange). NOE correlations were found between the phen proton H5 and acridine proton H7 (cf., Figure 1 for numbering), proving the proximity of the phen and acridine groups. X-ray crystallographic analysis of the crystals grown by layering diethyl ether on the solution resulting from the titration provided the molecular structure of the species formed and confirmed the incorporation of the guest between the two parallel acridine groups of the $\mathbf{WAcr_2}$ receptor in the U form (Figure 6). Two of the three rings of the phen unit are inserted inside the receptor cavity; the two phen nitrogen atoms take part in the zinc

(19) Padilla-Tosta, M. E.; Lloris, J. M.; Martínez-Máñez, R.; Pardo, T.; Soto, J. *Inorg. Chim. Acta* **1999**, *292*, 28−33.

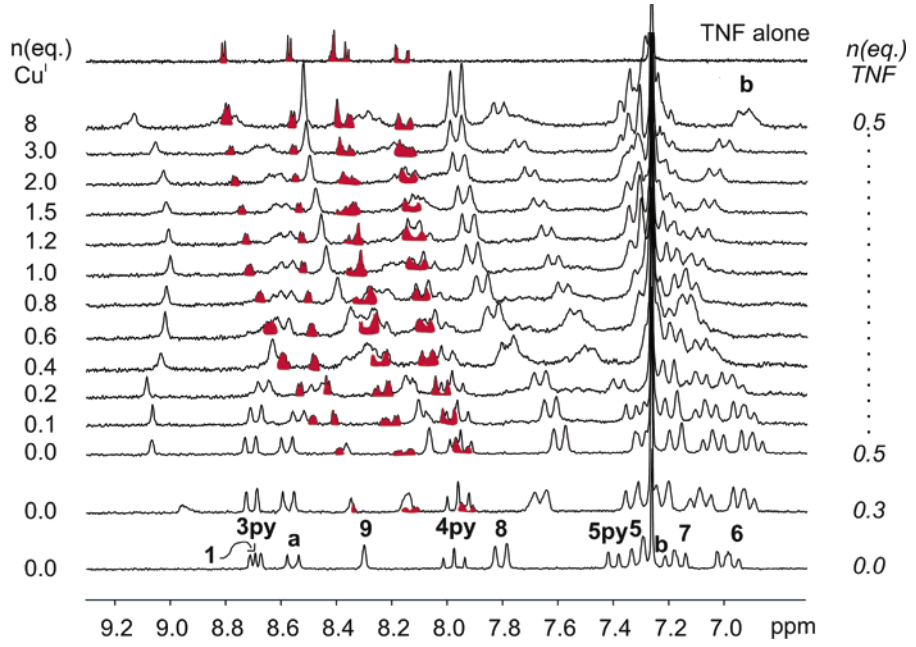

Figure 5. 200 MHz ^{1}H NMR spectral modifications on titration of $Cu(CH_3CN)_4$, BF_4 (16 mM solution in 2.0:1.0 $CDCl_3/CD_3CN$) into a solution of [TNF ⊂ $\mathbf{U_{Bu}Ant_2}$] (same mixture of solvents); to the free receptor (first spectrum at the bottom) were added up to 0.5 equiv of TNF (scale on the right-hand side), followed by the gradual addition of copper(I) salt solution (scale on the left-hand side). The spectrum of the free TNF guest in the same mixture of solvents is displayed at the top. The absolute values of the chemical shifts were referenced relative to the residual $CHCl_3$ signal (7.26 ppm).

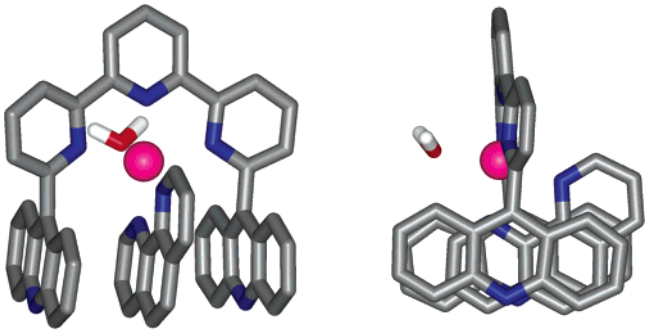

Figure 6. Face (a) and side (b) views of the mixed complex [phen ⊂ Zn^{II},$\mathbf{WAcr_2}$]·$2CF_3SO_3$ (noncoordinating solvent molecules and anions are omitted for clarity).

complexation, which picks up a water molecule to complete its distorted octahedral coordination sphere. The coordination of the phen substrate to the zinc cation effector strongly contributes to the formation of the sandwich complex and makes it difficult to assess the extent of donor/acceptor interaction between receptor and substrate.

Noncoordinating, electron-poor guests such as TNF and TCNQ (1 equiv) were therefore combined with the receptor, and zinc triflate was added under the same conditions as in the previously described experiment conducted with phen; no sign of interaction was detected by NMR or visually at millimolar concentrations. Because small cations such as zinc are known to induce pinching of the terpy frame (∼11°),[20a] which could prevent the intercalation of the guest between nonparallel planar binding sites, a larger cation such as lead(II), known to impose a smaller pinching angle (∼6°),[20b] was introduced, but no guest inclusion was observed, even with a stronger electron donor receptor ($\mathbf{WAnt_2}$, not described herein) and excess electron acceptor substrate (TCNQ).

As pinching appeared not to be the major factor responsible for the poor binding ability of the $\mathbf{Wax_2}$ receptors switched into their U-shaped conformation, we inferred that the cavity space between the two flat walls may be partially obstructed by the solvation sphere of the octahedral cation. To verify this hypothesis, we designed a new terpy-based ligand $\mathbf{W(CONHAnt)_2}$, where an amide spacer decouples the cation coordination and the guest binding processes by shifting the guest binding event further away from the cation effector. It also provides two additional coordination sites for the metal, the carbonyl oxygen atoms, which reduces the occupancy of the internal cavity by coordinating solvent molecules. This new ligand was poorly soluble in $CDCl_3$, CD_3CN, and their mixtures, preventing direct titration experiments with zinc triflate in the presence of guest. Nevertheless, the zinc complex [Zn^{II} ⊂ $\mathbf{W(CONHAnt)_2}$] formed by mixing the receptor, zinc triflate, and the solvent was very soluble in CD_3CN. It gave crystals suitable for X-ray crystallographic analysis. The molecular structure determined presented the expected U shape (Figure 7) with the zinc cation complexed in a very distorted octahedral geometry, involving the two amide oxygen atoms and a solvent molecule (acetonitrile; two of them appear in the crystal because of disorder). The coordination of the amide oxygen atoms contributes to a strong pinching (17.6°) of the scaffold, which brings the two anthracene substituents close enough for stacking $\pi-\pi$ interaction (6.6 Å).

When [Zn^{II} ⊂ $\mathbf{W(CONHAnt)_2}$] was titrated with TCNQ (or TNF) in CD_3CN, immediate green (or red) coloration accompanied the shielding of the NMR signals of the anthracene protons H8 and H9, attesting the formation of the expected charge-transfer complex, with a binding constant of approximately 100 M^{-1} for both guests (Table 1) in this solvent. The X-ray diffraction data obtained for the dark green crystals grown

(20) (a) Vlasse, M.; Rojo, T.; Beltran-Porter, D. *Acta Crystallogr., Sect. C: Cryst. Struct. Commun*. **1983**, *C39*, 560−563. (b) Engelhardt, L. M.; Harrowfield, J. M.; Miyamae, H.; Patrick, J. M.; Skelton, B. W.; Soudi, A. A.; White, A. H. *Aust. J. Chem.* **1996**, *49*, 1135−1146.

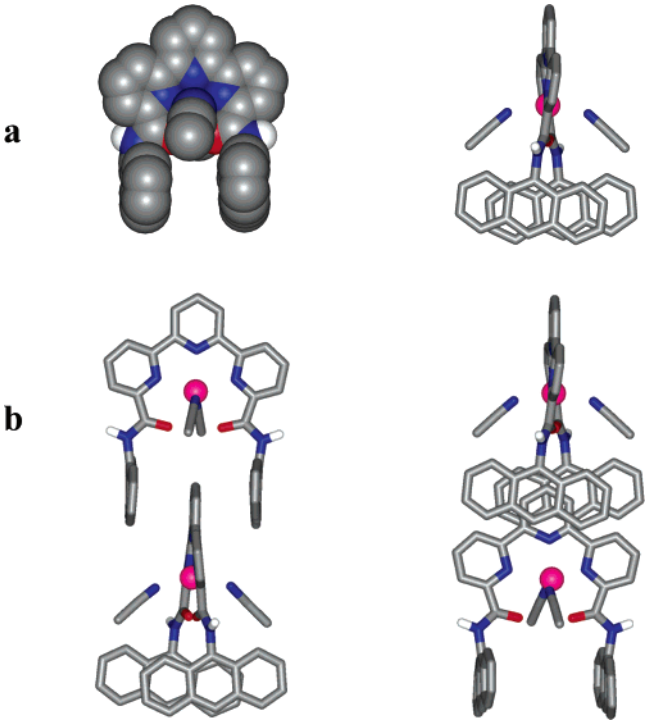

Figure 7. Crystal structure of the U-shaped receptor [Zn^{II} ⊂ **W-(CONHAnt)$_2$**]·$2CF_3SO_3$: (a) CPK (left) and ball-and-stick (right) representations of the face and side views of the isolated receptor, respectively; (b) ball-and-stick representation of two perpendicular views of a (dimeric) part of the 1D polymer formed by the self-assembly of the receptors in the solid state (noncoordinating solvent molecules and anions are omitted for clarity).

at the end of the TCNQ titration could not be refined to a sufficient extent for atomic resolution, but the raw data were good enough to ascertain that one molecule of TCNQ was located within the bis-anthracene cavity, and another one was located between two anthracenes belonging to two different complexes in the solid state (data not shown).

Affinity of Tweezer-type Receptors for Substrate Species. Py-pym-py System. As evidenced in the solid state as well as in solution, the **py-pym-py** sequence contains structural information that enforces a U-shaped conformation, appropriate for intercalative electron donor/acceptor complexation between its large aromatic 6,6″ substituents. A related family of compounds based on a **Ph-py-Ph** sequence (**Ph** = 1,3-substituted phenyl, **py** = 2,6-dibsubstituted pyridine) pointed to the importance of preorganization in such donor/acceptor complexes, the binding constants being typically divided by a factor of 4 for each allowed free rotation around the **Ph**−**py** bond in the **Ph-py-Ph** sequence.[18h,21] Although no direct comparison can be made between these two systems due to different substitution patterns and guests studied, the binding constants determined in the present report are higher than those one may anticipate with the **Ph-py-Ph** sequence. The binding constant of TNF with the covalently U-constrained **Acr-Ph′-py′-Ph′-Acr** receptor (in which the **Ph′** and **py′** are linked by an ethylene bridge between the phenyl 3 and the pyridine 3 positions) is only approximately 3 times higher than that with the **py-pym-py**-based $\mathbf{U_HAcr_2}$, instead of the 16-fold difference anticipated on the basis of the published data.[21] A higher preorganization of the **py-pym-py** sequence as compared to **Ph-py-Ph** could account for the better binding affinity, although it cannot compete with the covalently constrained scaffold.

Although an anthracene unit is a better donor, the acridine-containing tweezers offer more versatility, being able to complex electron acceptors in the neutral state (complexes with TCNQ and TNF, Table 1), but also electron donors when protonated or alkylated (complexes with TDOA, Table 1). The self-assembly of $\mathbf{U_HAcr_2Me^+}$ containing both donor and acceptor sites in the solid state, complemented by hydrogen bonding patterns (dashed lines, Figure 2, $\mathbf{c_2}$) to form a 1D polymer (Figure 2, $\mathbf{c_2}$), is an illustrative example of the versatility of these systems.

Py-py-py System. The 6,6″ disubstituted **py-py-py** sequence is only capable of guest binding when it is switched to a U shape by complexation of a cation such as zinc. The resulting conformation is then well preorganized for guest inclusion, provided that enough room is available for the guest to interact with the cavity walls. The different behaviors of $\mathbf{WAcr_2}$ and $\mathbf{W(CONHAnt)_2}$ are indicative of the necessity of taking into account the extra coordination sphere provided by the solvent. In $\mathbf{WAcr_2}$, the metal cation recruits solvent molecules to complete its coordination sphere, leaving little to no room for further guest inclusion, unless the guest simultaneously participates in cation coordination, as in [phen Zn^{II} ⊂ $\mathbf{WAcr_2}$] (Figure 6). The amide spacer provided in $\mathbf{W(CONHAnt)_2}$ is sufficient to decouple the two binding processes (cation coordination and acceptor intercalation), as evidenced by the formation of the expected charge-transfer complexes. Nevertheless, the binding constants measured for TNF and TCNQ inclusion in [Zn^{II} ⊂ $\mathbf{W(CONHAnt)_2}$] are approximately 1 order of magnitude smaller than those for the corresponding **py-pym-py** complexes (acetonitrile was used for the terpy-based receptor, a more polar solvent than chloroform, which should actually promote interactions such as stacking). This latter observation may find its explanation is a combination of factors. First, the positive charge on the receptor partner is expected to be nonoptimal for electron-poor substrate binding. Second, the presence of the metal in the vicinity of the complexing cavity gathers anion and solvent (inner and outer spheres) molecules which compete for cavity occupancy. Finally, the amide spacer may still impose some sort of steric hindrance (vide infra).

Features of the Switching Effector, the Metal Cation. Choice of the Binding Cations. In view of the nature of the ligands, soft cations are required for a good binding to nitrogen-containing ligands in organic-based solvents. Copper(I) is especially well suited in this respect, and zinc(II) is known for its affinity to N- and S-containing ligands in synthetic and natural systems.[4a]

Kinetic Features. As in the natural systems based on calcium- and zinc-controlled triggers,[4a] fast kinetics is crucial for the elaboration of dynamic operators. The fast exchange observed in the course of the Cu^I titration of the **py-pym-py** sequence attests that this condition is met. Although zinc complexation is slow on the NMR time scale, it is fast enough for the present study, as stable NMR signals are obtained right after salt addition.

Preferential Coordination Geometry. The **py-pym-py** sequence in a W conformation leaves little room for additional

(21) (a) Zimmerman, S. C.; VanZyl, C. M.; Hamilton, G. S. *J. Am. Chem. Soc.* **1989**, *111*, 1373−1381. (b) Zimmerman, S. C.; Mrksich, M.; Baloga, M. *J. Am. Chem. Soc.* **1989**, *111*, 8528−8530.

ligands on a metal ion coordinated to the bidentate bipy-type binding subunits, in particular when the 6 and 6″ positions are substituted with bulky groups such as anthracene and acridine. Cations of tetrahedral coordination geometry are therefore likely to better accommodate these bidentate sites than metals preferring higher coordination numbers or planar geometry. Copper(I) is known to preferentially bind to bipy-type units in a tetrahedral coordination geometry and to be protected from oxidation by substituents α to the nitrogen sites. The pyrimidine 2-aryl substituent probably provides additional protection to the required cuprous state. On the contrary, terpy offers a planar arrangement of three nitrogen donors, which can be accommodated by both octahedral and square planar coordinating metal ions. Zinc and lead cations are compatible with such complexation sites, present fast kinetics, and are diamagnetic.

Allosteric Regulation of Substrate Binding and Release. The structural switching processes between W and U states undergone by the present **py-pym-py** and **py-py-py** systems upon cation binding (Scheme 1), respectively, allow for substrate release and binding through an allosteric mechanism.[22]

The tridentate terpy ligand in $\mathbf{WAcr_2}$ leaves free three additional interactions around a bound octahedral cation, thus coupling conformational switching through cation coordination directly to substrate binding to the cation and intercalative "tweezing" of the substrate. The effector is then involved in a direct binding site regulation.

In $\mathbf{W(CONHAnt)_2}$, however, the coordinating amide spacer decouples cation and substrate binding, allowing for cation-induced allosteric regulation of the substrate binding process without direct connection of the substrate to the allosteric effector, the metal ion. The coordination sphere of the cation may nevertheless contribute indirectly to the regulation of substrate binding. The crystal structure of the receptor (Figure 7b) provides information concerning its ability to be involved in $\pi-\pi$ stacking interactions. In the solid state, the electron-deprived central pyridine (following zinc complexation) of one molecule is inserted between the two electron-rich anthracene substituents of another one. This pattern leads to the formation of a one-dimensional donor/acceptor polymer, in which the identical consecutive host and guest species are rotated by 90° relative to one another. The extent of penetration of the terpy scaffold inside the cavity of the neighboring receptor is limited by the interaction of the proton in position 4 of the central pyridine of the guest and the two amide oxygen atoms of the host, which belong to the cation binding site and may interfere with the electron acceptor substrates in solution as well.

In the **py-pym-py** sequence, the peripheral localization of the copper(I) effector with respect to the substrate binding pocket provides purely allosteric regulation. The cation coordination in a region "remote" from the substrate binding site provokes a rotational movement that modifies the interaction of the receptor with the substrate. This is reminiscent of the calcium binding regulation of proteins such as calmodulin and troponin C, which provides a trigger for a variety of chemical and mechanical processes.[4] In these ubiquitous proteins, calcium binding to the carboxylate-rich EF-hand subdomain, remote from the active site, induces the rotational and lateral relative movements of the flanking helices, a process which lies at the heart of the calcium-induced regulation. The function of the $\mathbf{U_yAx_2}$ tweezers, which release substrate upon copper(I) binding, is itself analogous to the calcium-induced release of vesicular contents by annexins in cells.[4a,b]

Molecular Switching Processes. Numerous natural conformational switches, such as retinal and calcium binding subdomains, are involved in a two-state process (cis/trans, bound/not bound), resulting in a 0 or 1 response. Such is the case for the **py-py-py** sequence described herein, in which the coordination of 1 equiv of zinc(II) provokes the rotation of two bonds and switches the terpyridine-based ligand from a W to a U shape in a single step process, embodying a two-state W/U molecular switch (Scheme 1, top).

The **py-pym-py** sequence requires the coordination of two copper(I) atoms to complete full conversion from a U to a W shape. In principle, binding of the first metal ion leads to an intermediate S state, in which only one of the **py−pym** bonds is rotated (Scheme 1, bottom; central form in Figure 1a). Experimentally, the binding of the two copper atoms is anticooperative, as evidenced by the NMR titration of $\mathbf{U_{Bu}Acr_2}$ with $Cu(CH_3CN)_4$, BF_4 in 1.0:1.0 $CDCl_3/CD_3CN$ (data not shown). The titration data up to 2.0 equiv of added titrant could be best fitted as a 1:1 complex, with a $\log(K_{assoc})$ of 2.93 ± 0.07, indicating that the binding of the second effector cation is much weaker. This latter point is illustrated in Figure 5, where the signals of the receptor still evolve after 8 equiv of Cu^I have been added. ESMS measurements (data not shown) confirmed that the 1:1 complex is largely predominant after addition of 2.0 equiv of Cu^I, giving way to the 2:1 adduct only when excess Cu^I (>8 equiv) is added. This anticooperative behavior may be explained by electrostatic repulsion together with the even poorer ligand ability of the central pyrimidine once a first cation binds to one of its nitrogen atoms, weakening the basicity of the second nitrogen coordination site. It complements the parallel between this system and calcium-dependent proteins such as proteinase K.[4c] Such anticooperative binding of the two Cu^I effectors provides therefore a wide range of copper concentrations in which the S shape is the predominant species and makes in effect the **py-pym-py** sequence an ion-controlled three-state W/S/U molecular switch. Because of their obvious richness, multistate molecular switches have attracted much attention. Such molecular systems based on photoinduced chiral control,[23a] liquid crystal properties,[23b] photo- and ion-controlled spectroscopic properties,[24] as well as electro-controlled shuttling[25] involving multiple states open a very promising field.

Conclusion

The present results illustrate the design of two conformational switches of complementary behavior in ion-regulated substrate binding. The bistable **py-py-py**-based receptor converts from a W to a U shape upon cation complexation, the latter being capable of substrate binding by insertion between the branches of the tweezer, with the participation of the cation effector in the substrate binding event depending on the terpy substitution motif. Conversely, the coordination of copper(I) cations to the

(22) Shinkai, S.; Ikeda, M.; Sugasaki, A.; Takeuchi, M. *Acc. Chem. Res.* **2001**, *34*, 494−503. Rebek, J., Jr. *Acc. Chem. Res.* **1984**, *17*, 258−264.

(23) (a) Koumura, N.; Zijistra, R. W. J.; van Delden, R. A.; Harada, N.; Feringa, B. L. *Nature* **1999**, *401*, 152−155. (b) Huck, N. P. M.; Jager, W. F.; de Lange, B.; Feringa, B. L. *Science* **1996**, *273*, 1686−1688.

(24) Maesri, M.; Pina, F.; Balzani, V. In *Molecular Switches*; Feringa, B., Ed.; Wiley-VCH: Weinheim, 2001; pp 309−337.

(25) Cárdenas, D. J.; Livoreil, A.; Sauvage, J.-P. *J. Am. Chem. Soc.* **1996**, *118*, 8, 11980−11981.

py-pym-py sequence provokes the release of an intercalated substrate, by inducing a conformational change from a U to a W shape, via an S-shaped intermediate, in a three-stage tristable allosteric mechanism.

The latter sequence is an example of a multistate supramolecular switching device, a promising area which paves the way to complex nanomechanical chemical systems. Further developments in this direction are currently under investigation in our laboratory and will be reported in due course.

Experimental Section

General Methods. The **py-pym-py** and **py-py-py** receptors were obtained by standard palladium-catalyzed coupling and amide bond formation using acyl chlorides as activating species and were characterized by ^{1}H (200 MHz unless specified otherwise) and ^{13}C (when solubility permitted; 50 MHz unless specified otherwise) NMR spectroscopy, mass spectrometry (performed in the Laboratoire de Spectrométrie de masse Bio-organique, Université Louis Pasteur), and elemental analyses (performed by the Service de Microanalyses, Université Louis Pasteur). Technical 9-nitroanthracene (Lancaster) was purified by silica gel chromatography (hexane/ethyl-acetate 2.0:0.2 to 2.0:1.0), and 7,7′,8,8′-tetracyanoquinodimethane was recrystallized (ethyl acetate) before use. All other reagents were used as received. Dry solvents (1,2-dichloroethane, toluene) were distilled on drying agents (calcium hydride, Na, respectively) under argon.

9-(6-Trimethylstannyl-pyridin-2-yl)-acridine (Acr-py-Sn). To 4.9 mmol of 2,6-bis-(trimethylstannyl)pyridine[26] solubilized in 32 mL of freshly distilled toluene were added 1.05 g of 9-chloroacridine[27] (4.9 mmol, 1.0 equiv) and 288 mg of tetrakistriphenylphosphinepalladium-(0) (0.25 mmol, 0.05 equiv). The solution was purged with argon, protected from light, and refluxed under argon. An additional 100 mg of catalyst was added after 12 h, and the solution was refluxed for a further 5 h. At room temperature, the mixture was evaporated onto basic alumina (activity I), run through a short alumina column (hexane/Et_2O 3.0:0.2, $R_f = 0.34$), and concentrated in vacuo to give a yellow solid (yield: 60%).

2-(4-*n*-Butylphenyl)-4,6-bis-(6-(acrid-9-yl)-pyridin-2-yl)-pyrimidine ($U_{Bu}Acr_2$). To 3.2 mmol of **Acr-py-Sn** (2.24 equiv) suspended in 10 mL of DMF were added 402 mg of 2-(4-*n*-butylphenyl)-4,6-dichloropyrimidine[13c] (1.43 mmol) and 50 mg of dichlorobistriphenylphosphinepalladium(II) (7.1×10^{-5} mol, 0.05 equiv). The solution was purged with argon, protected from light, and heated at 90 °C under argon for 18 h. After concentration under vacuum, the greenish solid was taken up in dichloromethane (120 mL) and washed with water (20 mL) and brine (10 mL). The organic layer was dried (Na_2SO_4), filtered, concentrated, adsorbed onto basic alumina, and washed (hexane/Et_2O 4:1, Et_2O, Et_2O/CH_3OH 10%). The product was then eluted with chloroform and recrystallized (chloroform, hexane, ether) to yield 434 mg (42%) of a pale yellow solid. ^{1}H NMR ($CDCl_3$): 9.03 (s, 1H), 8.80 (d, $^3J = 7.9$ Hz, 2H), 8.73 (d, $^3J = 8.2$ Hz, 2H), 8.23 (d, $^3J = 8.5$ Hz, 4H), 8.12 (t, $^3J = 7.8$ Hz, 2H), 7.55−7.7 (m, 10H), 7.44 (d, $^3J = 8.2$ Hz, 2H), 7.12 (t, $^3J = 7.9$ Hz, 4H), 2.77 (t, $^3J = 7.6$ Hz, 2H), 1.73 (quint, $^3J = 7.8$ Hz, 2H), 1.41 (sext, $^3J = 7.8$ Hz, 2H), 1.00 (t, $^3J = 7.4$ Hz, 3H). ^{13}C NMR ($CDCl_3$): 164.4, 155.4, 155.2, 148.7, 146.2, 137.3, 135.4, 130.0, 129.5, 128.8, 128.4, 127.9, 126.1, 126.0, 124.5, 121.2, 112.6, 35.7, 33.6, 22.4, 14.0. R_f (SiO_2, CH_2Cl_2/CH_3OH 2.0:0.1) = 0.21. Fp > 260 °C. FAB+: 721.3 (MH^+). UV−vis: λ_{max} abs (log ϵ): 254 (5.09), 279 (4.38), 330 (4.16), 344 (4.23), 361 (4.30), 387 (4.0). Fluo: λ_{max} em = 421 nm. Anal. Calcd for $C_{50}H_{36}N_6$·0.10$CHCl_3$: C, 82.12; H, 4.97; N, 11.47. Found: C, 82.09; H, 4.83; N, 11.50.

4,6-Bis-(6-(acrid-9-yl)-pyridin-2-yl)-pyrimidine (U_HAcr_2). The same methodology as above was applied starting from unsubstituted 4,6-dichloropyrimidine to yield **U_HAcr_2** as a pale yellow solid (30%). ^{1}H NMR ($CDCl_3$): 9.47 (d, $J = 1.2$ Hz, 1H), 9.17 (d, $J = 1.2$ Hz, 1H), 8.62 (dd, $^3J = 7.6$ Hz, 2H), 8.24 (d, $^3J = 8.5$ Hz, 4H), 8.11 (t, $^3J = 7.8$ Hz, 2H), 7.55−7.7 (m, 10H), 7.15 (td, $^3J = 7.9$ Hz, 4H). ^{13}C NMR ($CDCl_3$): 164.1, 155.5, 154.7, 154.3, 148.8, 145.1, 143.8, 137.5, 129.9, 129.7, 128.0, 125.9, 124.5, 121.2, 115.3. R_f (SiO_2, CH_2Cl_2/CH_3OH 2.0:0.2) = 0.20. Fp > 260 °C. FAB+: 589.1 (MH^+). UV−vis (CH_2Cl_2): λ_{max} abs (log ϵ): 252 (5.3), 293 sh. (4.3), 348 (4.2), 361 (4.3), 384 (4.0). Fluo (CH_2Cl_2): λ_{max} em = 440 nm. Anal. Calcd for $C_{40}H_{24}N_6$·0.24$CHCl_3$: C, 78.29; H, 3.96; N, 13.61. Found: C, 78.30; H, 3.92; N, 13.71.

2-(4-*n*-Butylphenyl)-4,6-bis-(6-(10-*N*-methylacrid-9-ylinium)-pyridin-2-yl)-pyrimidine Bistriflate ($U_{Bu}Acr_2Me_2$, 2TfO). To 36 mg of bisacridine **$U_{Bu}Acr_2$** (5.0×10^{-5} mol) solubilized in 17 mL of hot dry 1,2-dichloroethane was added 13 μL of methyl triflate under argon. Another 4.5 μL of methyl triflate (3.1 total equiv) was added after refluxing for 6 h, and heating was continued for an additional hour. Diethyl ether (5 mL) was added at room temperature, and the precipitate was filtered, washed twice with diethyl ether (2 mL), and dried in vacuo to yield 51 mg of a bright yellow solid (98%). ^{1}H NMR (CD_3OD, 500 MHz, 5 mM): 8.71 (d, $^3J = 8.0$ Hz, 2H), 8.67 (s, 1H), 8.35 (d, $^3J = 9.3$ Hz, 4H), 8.27 (td, $^3J = 9.1$ Hz, $^4J = 1.2$ Hz, 4H), 7.89 (d, $^3J = 7.8$ Hz, 2H), 7.81−7.85 (m, 4H), 7.33−7.40 (m, 6H), 7.18 (d, $^3J = 8.3$ Hz, 4H), 4.38 (s, 6H), 8.71 (t, $^3J = 8.0$ Hz, 2H), 1.98 (quint, $^3J = 7.8$ Hz, 2H), 1.67 (sext, $^3J = 7.4$ Hz, 2H), 1.17 (t, $^3J = 7.4$ Hz, 2H). ^{13}C NMR (CD_3OD, 125 MHz, 5 mM): 163.3, 161.9, 158.2, 154.6, 153.0, 149.7, 142.2, 140.5, 139.5, 135.0, 131.3, 130.3, 129.7, 128.9, 128.1, 126.4, 122.7, 120.0, 113.8, 39.3, 37.0, 34.9, 23.8, 14.5. R_f (SiO_2, CH_2Cl_2/CH_3OH 2.0:0.3) = 0.30. HR-FAB+: $(C_{53}H_{42}N_6F_3SO_3)^+$ calc. 899.2992; obs. 899.2991. UV−vis (CH_2Cl_2): λ_{max} abs (log ϵ): 263 (5.0), 300 (4.2), 347 (4.2), 363 (4.4), 412 (3.9), 427 (3.9), 453 (3.7). Fluo (CH_2Cl_2): λ_{max} em = 511, 527 nm.

2-Anthracen-9-yl-4,4,5,5-tetramethyl-[1,3,2]-dioxaborolane (Ant-B(OR)$_2$). To 4.00 g of commercially available 9-bromoanthracene (15.6 mmol) suspended in 25 mL of freshly distilled toluene were added 540 mg of dichlorobistriphenylphosphinepalladium(II) (7.7×10^{-4} mol, 0.05 equiv), 6.4 mL of triethylamine (46 mmol, 2.9 equiv), and 3.5 mL of pinacolborane (24 mmol, 1.5 equiv) under argon. The solution was refluxed for 16 h under argon, after which it was washed with water (30 mL), filtered through Celite, washed again with water (30 mL), and concentrated. The residue was taken up in dichloromethane (15 mL) and filtered through a short silica gel column. The yellow eluate was concentrated and recrystallized from hexane (300 mL) to yield 3.5 g of yellow crystals (74%). ^{1}H NMR ($CDCl_3$): 8.51 (d, $^3J = 8$ Hz, 2H), 8.50 (s, 1H), 8.0 (m, 2H), 7.45−7.6 (m, 4H), 1.61 (s, 12H). ^{13}C NMR ($CDCl_3$): 135.9, 131.2, 129.5, 128.8, 128.3, 125.8, 125.3, 124.9, 84.3, 25.2. Fp = 138−140 °C. FAB+: 304.1 (MH^+). Anal. Calcd for $C_{20}H_{21}BO_2$: C, 78.97; H, 6.96; B, 3.55; O, 10.52. Found: C, 78.64; H, 6.87.

2-Anthracen-9-yl-6-bromopyridine (Ant-py-Br). First, 3.30 g of **Ant-B(OR)$_2$** (10.8 mmol), 7.74 g of 2,6-dibromopyridine (32.7 mmol, 3.0 equiv), 10.59 g of barium hydroxide octahydrate (33.6 mmol, 3.1 equiv), and 626 mg of tetrakistriphenylphosphinepalladium(0) (5.4×10^{-4} mol, 0.05 equiv) were suspended in a degassed mixture of toluene (330 mL) and water (6.6 mL) and refluxed under argon. After 14 h, additional water (3 mL), barium hydroxide (11.3 mmol, 1.0 equiv), 2,6-dibromopyridine (5.00 g, 21.1 mmol, 1.95 equiv), and catalyst (220 mg, 1.9×10^{-4} mol, 1.8×10^{-2} equiv) were added, and the mixture was brought back to reflux for another 22 h. The volatiles were then evaporated, and the residue was taken up in dichloromethane (400 mL) and water (100 mL). After filtration, the organic layer was washed with water (100 mL), brine (50 mL), dried (Na_2SO_4), filtered, concentrated, purified on silica gel (hexane/CH_2Cl_2 2.0:0.5 to CH_2Cl_2), and recrystallized (CH_2Cl_2/hexane) to yield 2.84 g (79%) of bright

(26) Yamamoto, Y.; Yanagi, A. *Bull. Chem. Soc. Jpn.* **1982**, *30*, 1731−1737.
(27) El-Sherief, H. A. H.; Abdel-Rahman, A. E.; Mahmoud, A. M. *J. Indian Chem. Soc.* **1983**, *LX*, 55−57.

yellow crystals. ^{1}H NMR ($CDCl_3$): 8.55 (s, 1H), 8.05 (d, ^3J = 8.5 Hz, 2H), 7.79 (t, ^3J = 7.5 Hz, 1H), 7.67 (d, ^3J = 7.8 Hz, 1H), 7.54 (d, ^3J = 8.0 Hz, 2H), 7.35−7.55 (m, 5H). ^{13}C NMR ($CDCl_3$): 159.4, 142.2, 138.6, 133.2, 131.2, 130.0, 128.5, 128.1, 126.8, 126.2, 125.8, 125.7, 125.2. Fp = 176 °C. FAB+: 304.1 (MH^+). Anal. Calcd for $C_{19}H_{12}$-NBr: C, 68.28; H, 3.62; N, 4.19; Br, 23.91. Found: C, 68.46; H, 3.65; N, 3.93.

2-Anthracen-9-yl-6-trimethylstannylpyridine (Ant-py-Sn). To 0.70 g of hexamethylditin (2.14 mmol, 1.2 equiv) solubilized in 14 mL of distilled toluene were added 609 mg of **Ant-py-Br** (1.82 mmol) and 117 mg of tetrakistriphenylphosphinepalladium(0) (1.0×10^{-4} mol, 0.05 equiv), and the solution was refluxed under argon for 1.5 h. After concentration of the dark solution, ^{1}H NMR allowed for the estimation that the crude contained 1.7 mmol of the desired stannane (93%), and was used as such in the following steps. ^{1}H NMR ($CDCl_3$): 8.52 (s, 1H), 8.04 (d, ^3J = 7.7 Hz, 2H), 7.73 (t, ^3J = 7.5 Hz, 1H), 7.67 (d, ^3J = 8.0 Hz, 2H), 7.61 (dd, ^3J = 8.0 Hz, ^4J = 1.2 Hz, 1H), 7.3−7.5 (m, 3H), 0.37 (s, 9H).

4,6-Bis-(6-anthracen-9-yl-pyridin-2-yl)-pyrimidine (U_HAnt_2). First, 6.1×10^{-4} mol of **Ant-py-Sn**, 43 mg of 4,6-dichloropyrimidine (2.89×10^{-4} mol), and 11 mg of tetrakistriphenylphosphinepalladium(0) (1.5×10^{-5} mol, 0.05 equiv) solubilized in 5 mL of DMF were degassed, protected from light, and heated at 100 °C under argon for 17 h. Most of the DMF was evaporated in vacuo, and the brown residue was washed with methanol, purified by column chromatography on basic alumina (hexane/CH_2Cl_2 2.0:1.5 to CH_2Cl_2 alone), and recrystallized ($CHCl_3$/Et_2O) to yield 32 mg of thin yellow needles (19%). ^{1}H NMR ($CDCl_3$): 9.46 (d, J = 1.2 Hz, 1H), 9.13 (d, J = 1.1 Hz, 1H), 8.53 (dd, ^3J = 7.9 Hz, 2H), 8.48 (s, 2H), 8.04 (t, ^3J = 7.8 Hz, 2H), 7.98 (d, ^3J = 8.6 Hz, 4H), 7.5−7.6 (m, 6H), 7.33 (t, ^3J = 7.5 Hz, 4H), 7.1 (td, ^3J = 8 Hz, 4H). R_f (Al_2O_3, hexane/CH_2Cl_2 1.0:1.0) = 0.36. Fp > 260 °C. EI: 293.7 (M^{2-}), 586.4 (M^-). UV−vis (CH_2Cl_2): λ_{max} abs (log ϵ): 250 (5.4), 256 (5.5), 298 (4.4), 332 (4.0), 349 (4.2), 366 (4.4), 386 (4.3). Fluo (CH_2Cl_2): λ_{max} em = 430, 510 nm. Anal. Calcd for $C_{42}H_{26}N_4$·0.23$CHCl_3$: C, 83.67; H, 4.40; N, 9.24. Found: C, 83.64; H, 4.38; N, 9.22.

4,6-Bis-(6-anthracen-9-yl-pyridin-2-yl)2-(4-*n*-butylphenyl)-pyrimidine ($U_{Bu}Ant_2$). This compound was obtained by a similar protocol, yielding the desired product as thin yellow needles (18%) after column chromatography and recrystallization. ^{1}H NMR ($CDCl_3$): 8.99 (s, 1H), 8.73 (d, ^3J = 8.0 Hz, 4H), 8.48 (s, 2H), 8.08 (t, ^3J = 7.8 Hz, 2H), 7.98 (d, ^3J = 8.4 Hz, 4H), 7.6 (d, ^3J = 8.1 Hz, 4H), 7.57 (d, ^3J = 7 Hz, 2H), 7.43 (d, ^3J = 8,0 Hz, 2H), 7.33 (t, ^3J = 7.5 Hz, 4H), 7.09 (t, ^3J = 7 Hz, 4H), 2.77 (t, ^3J = 7.6 Hz, 2H), 1.72 (quint, ^3J = 7.8 Hz, 2H), 1.43 (sext, ^3J = 7.8 Hz, 2H), 0.98 (t, ^3J = 7.4 Hz, 3H). R_f (Al_2O_3, hexane/CH_2Cl_2 2.0:1.0) = 0.30. Fp > 260 °C. FAB+: 719.3 (MH^+). UV−vis (CH_2Cl_2): λ_{max} abs (log ϵ): 250 (5.6), 256 (5.7), 280 (5.0), 332 (4.5), 348 (4.6), 366 (4.6), 386 (4.6). Fluo (CH_2Cl_2): λ_{max} em = 490 nm. Anal. Calcd for $C_{52}H_{38}N_4$·0.44$CHCl_3$: C, 81.65; H, 5.02; N, 7.26. Found: C, 81.62; H, 5.02; N, 7.23.

6,6″-Diacridin-9-yl-[2,2′;6′,2″]terpyridine ($WAcr_2$). A solution containing 2.5 mmol of **Acr-py-Sn**, 283 mg of 2,6-dibromopyridine (1.19 mmol), and 57 mg of tetrakistriphenylphosphinepalladium(0) (4.9×10^{-5} mol, 0.04 equiv) in 50 mL of distilled toluene was refluxed under argon for 12 h protected from light. After evaporation of the toluene, the yellow residue was washed with methanol and recrystallized ($CHCl_3$/CH_3OH), to yield 560 mg of a pale yellow solid (80%). ^{1}H NMR ($CDCl_3$): 8.93 (dd, ^3J = 7.9 Hz, ^4J = 0.9 Hz, 2H), 8.43 (d, ^3J = 7.9 Hz, 2H), 8.33 (dd, ^3J = 9 Hz, ^4J = 0.9 Hz, 4H), 8.12 (t, ^3J = 7.8 Hz, 2H), 7.7−7.9 (m, 9H), 7.61 (dd, ^3J = 7.6 Hz, ^4J = 0.9 Hz, 2H), 7.48 (td, ^3J = 8.2 Hz, ^4J = 1.2 Hz, 4H). ^{13}C NMR ($CDCl_3$): 156.7, 155.2, 149.0, 144.8, 138.1, 137.3, 130.1, 129.8, 126.4, 126.1, 124.8, 121.9, 120.5. R_f (SiO_2, CH_2Cl_2/CH_3OH 3.0:0.1) = 0.44. Fp = 190 °C (dec). HR-FAB+: ($C_{41}H_{25}N_5$)H^+ calc. 588.2188; obs. 588.2182. UV−vis (CH_2Cl_2): λ_{max} abs (log ϵ): 253 (5.4), 290 sh (4.3), 351 (4.2), 360 (4.3), 384 (4.1). Fluo (CH_2Cl_2): λ_{max} em = 434 nm. Anal Calcd for $C_{41}H_{25}N_5$·0.45$CHCl_3$: C, 77.67; H, 4.00; N, 10.93. Found: C, 77.68; H, 4.24; N, 11.33.

[2,2′;6′,2″]Terpyridine-6,6″-dicarboxylic Acid Diethylester [$W(CO_2Et)_2$]. First, 13 mmol of 2,6-bis-(trimethylstannyl)pyridine,[26] 7.27 g of 6-bromopyridine-2-carboxylic acid ethylester[28] (32 mmol, 2.4 equiv), and 610 mg of tetrakistriphenylphosphinepalladium(0) (5.3×10^{-4} mol, 0.04 equiv) solubilized in toluene (160 mL) were purged with argon and refluxed for 16 h. After evaporation of the solvent, the solid residue was taken up in dichloromethane (100 mL), filtered onto Celite, treated with decolorizing charcoal, concentrated, and recrystallized (CH_2Cl_2/Et_2O) to yield 2.28 g (46%) of the desired diester as a white solid. ^{1}H NMR ($CDCl_3$): 8.80 (dd, ^3J = 7.9 Hz, ^4J = 1.1 Hz, 2H), 8.65 (d, ^3J = 7.8 Hz, 2H), 8.16 (dd, ^3J = 8 Hz, 2H), 8.01 (t, ^3J = 7.8 Hz, 1H), 8.00 (t, ^3J = 7.8 Hz, 2H), 4.52 (quadr, ^3J = 7.1 Hz, 4H), 1.49 (t, ^3J = 7.1 Hz, 6H). ^{13}C NMR ($CDCl_3$): 165.3, 156.3, 154.5, 147.9, 138.2, 137.8, 125.0, 124.1, 122.1, 61.9, 14.4. R_f (Al_2O_3, CH_2Cl_2) = 0.19. Fp = 180 °C. FAB+: 377.3 (MH^+), 305.3 [(M − CO_2-Et)H^+], 231.2 [(M − 2CO_2Et)H^+]. Anal. Calcd for $C_{21}H_{19}N_3O_4$·0.06CH_2Cl_2: C, 66.13; H, 5.04; N, 10.99; O, 16.81. Found: C, 66.15; H, 4.80; N, 11.28.

[2,2′;6′,2″]Terpyridine-6,6″-dicarboxylic Acid [$W(CO_2H)_2$]. To 265 mg of **$W(CO_2Et)_2$** (7.02 mmol) suspended in a mixture of pyridine (10 mL) and water (5 mL) was added 1.0 mL of KOH 10% in methanol. The mixture was heated at 75 °C for 10 h. The solution was then filtered and acidified (pH ≈ 1) with concentrated HCl. The precipitate was centrifuged, washed with copious water, and dried in vacuo on phosphorus pentoxide, yielding 223 mg of a white powder (98%). ^{1}H NMR (DMSO-d_6): 8.87 (dd, ^3J = 7.3 Hz, ^4J = 1.5 Hz, 2H), 8.65 (d, ^3J = 7.9 Hz, 2H), 8.1−8.3 (m, 5H). ^{13}C NMR (DMSO-d_6): 165.9, 154.9, 154.0, 147.9, 138.8, 124.9, 123.8, 121.6. Fp > 260 °C (dec). ESMS+: 320.0 (MH^+). Anal. Calcd for $C_{17}H_{11}N_3O_4$·0.5H_2O: C, 61.82; H, 3.66; N, 12.72; O, 21.80. Found: C, 61.74; H, 3.74; N, 12.76.

[2,2′;6′,2″]Terpyridine-6,6″-dicarboxylic Acid Bisanthracen-9-ylamide [$W(CONHAnt)_2$]. First, 197 mg of diacid **$W(CO_2H)_2$** (6.1 mmol) suspended in 2.0 mL of freshly distilled thionyl chloride was refluxed for 3 h under argon. Most of the solvent was evaporated and then coevaporated with 3 × 1 mL of dry dichloromethane. The crude diacyl chloride obtained was then suspended in 3 mL of dry dichloromethane, and 295 mg of 9-aminoanthracene[29] (15 mmol, 2.5 equiv) was added as a solid. The mixture was refluxed for 4 h, concentrated, and taken up in fresh dichloromethane. The yellow precipitate was then filtered, successively washed with chloroform, water, and ethanol, solubilized in pyridine, and slowly precipitated by ethanol diffusion, yielding 302 mg of a shiny beige solid (74%). ^{1}H NMR (pyridine-d_5): 11.88 (br s, 2H), 9.25 (dd, ^3J = 8.0 Hz, ^4J = 1.1 Hz, 2H), 8.94 (d, ^3J = 8.0 Hz, 2H), 8.8 (2H in the solvent signal), 8.70 (br d, ^3J = 7.7 Hz, 4H), 8.61 (s, 2H), 8.39 (t, ^3J = 8.4 Hz, 1H), 8.39 (t, ^3J = 7.7 Hz, 2H), 7.5−7.5 (m, 8H). Fp > 260 °C (dec). FAB+: 672.3 (MH^+). Anal. Calcd for $C_{45}H_{29}N_5O_2$·0.38H_2O: C, 79.65; H, 4.42; N, 10.32; O, 6.51. Found: C, 79.64; H, 4.26; N, 10.30.

Spectroscopic Measurements. UV−vis and fluorescence spectra were recorded on a Varian CARY 13e spectrometer at 25 °C and an AMINCO-Bowman Series 2 fluorimeter at 25 °C, respectively, using degassed spectrograde or freshly distilled solvents. NMR characterization and studies were carried out on a Bruker AC 200 spectrometer at 25 °C unless otherwise specified. For ^{1}H NMR titrations, determined volumes of a solution of the titrant (guest or salt solution) of known concentration (typically 10−25 mM) in a solvent or mixture of solvents were added to a solution of the receptor (typically 2−5 mM) in the same mixture of solvent, and the chemical shift of all protons was monitored. Those that were most affected by the binding event were used to determine the binding constant and stoichiometry using Chem Equili software (version 6.1, 1998, V. P. Solov'ev, Moscow University),

(28) Funeriu, D. P.; Lehn, J.-M.; Baum, G.; Fenske, D. *Chem.-Eur. J.* **1997**, *3*, 99−104.
(29) Messenheimer, J. *Ber.* **1900**, *33*, 3547−3549.

confirming the consistency of the results using all three Monte Carlo, simplex, and gradient iterative methods.

X-ray Crystallography. Single crystals suitable for X-ray analysis were obtained by slow diffusion of a poor solvent (diethyl ether, cyclohexane) into concentrated solutions, except for **U_HAcr$_2$Me, TfO** which crystallized directly out of chloroform. The data were recorded on a NONIUS KappaCCD diffractometer at 173 K (except for **U_HAcr$_2$** and **U_{Bu}Acr$_2$H$_2$, 2C$_2$F$_3$O$_2$** both analyzed at 100 K), in the laboratoire de Cristallochimie Structurale (Louis Pasteur University, Strasbourg, France). The structures were solved by Richard G. Khoury [**U_HAcr$_2$, (U_{Bu}Acr$_2$H$_2$, 2C$_2$F$_3$O$_2$), (U_HAcr$_2$Me, TfO**)], Nathalie Kyritsakas, and André De Cian {(TNF ⊂ **U_HAnt$_2$**), (phen ⊂ Zn^{II}, **Wacr$_2$**), [(Zn^{II} ⊂ **W(CONHAnt)$_2$**]} using (Bruker) SAINT and SHELXTL 97 software.

Single crystals of **U_HAcr$_2$** [$C_{40}H_{24}N_6$] were grown by slow diffusion of diethyl ether into a chloroform solution. Crystals were placed in oil, and a single colorless crystal of dimensions 0.27 × 0.16 × 0.14 mm was mounted on a glass fiber and placed in a low-temperature N_2 stream. The cell was monoclinic with a space group of *C*2/*c*. Cell dimensions: $a = 26.825$ Å, $b = 11.593$ Å, $c = 9.322$ Å, $\alpha = \gamma = 90°$, $\beta = 93.60°$, $V = 2893.4$, and $Z = 4$ (FW = 588.65 and $\rho = 1.351$ g/cm^{-3}). Reflections were collected $1.91° \leq \theta \leq 27.49°$ for a total of 3234 of which 1670 were unique, having $I > 2\sigma(I)$; the number of parameters is 209. Final *R* factors were $R_1 = 0.0551$ (based on observed data) and w$R_2 = 0.1739$ (based on all data), GOF = 0.839, maximal residual electron density is 0.188 e Å^{-3}.

Single crystals of **U_{Bu}Acr$_2$H$_2$**·2CF_3CO_2 [$C_{50}H_{38}N_6$·2$C_2F_3O_2$·2$CHCl_3$·0.5C_6H_{12}] were grown by slow diffusion of cyclohexane into a chloroform solution. Crystals were placed in oil, and a single colorless crystal of dimensions 0.16 × 0.10 × 0.05 mm was mounted on a glass fiber and placed in a low-temperature N_2 stream. The cell was triclinic with a space group of *P*-1. Cell dimensions: $a = 13.310$ Å, $b = 13.490$ Å, $c = 16.660$ Å, $\alpha = 81.15°$, $\beta = 74.62°$, $\gamma = 80.74°$, $V = 2827.1$, and $Z = 4$ (FW = 1229.76 and $\rho = 2.046$ g/cm^{-3}). Reflections were collected $1.60° \leq \theta \leq 20.81°$ for a total of 5860 of which 4752 were unique, having $I > 2\sigma(I)$; number of parameters is 736. Final *R* factors were $R_1 = 0.1171$ (based on observed data) and w$R_2 = 0.3282$ (based on all data), GOF = 1.080, maximal residual electron density is 0.732 e Å^{-3}.

Single crystals of **U_HAcr$_2$Me**·CF_3SO_3 [$C_{41}H_{27}N_6$·CF_3SO_3] were grown by slow evaporation of a chloroform solution. Crystals were placed in oil, and a single orange crystal of dimensions 0.24 × 0.21 × 0.14 mm was mounted on a glass fiber and placed in a low-temperature N_2 stream. The cell was triclinic with a space group of *P*-1. Cell dimensions: $a = 11.161$ Å, $b = 13.733$ Å, $c = 14.107$ Å, $\alpha = 67.50°$, $\beta = 74.02°$, $\gamma = 71.86°$, $V = 1868.2$, and $Z = 2$ (FW = 752.76 and $\rho = 1.338$ g/cm^{-3}). Reflections were collected $1.59° \leq \theta \leq 27.54°$ for a total of 8449 of which 4543 were unique, having $I > 2\sigma(I)$; number of parameters is 485. Final *R* factors were $R_1 = 0.1739$ (based on observed data) and w$R_2 = 0.3604$ (based on all data), GOF = 1.697, maximal residual electron density is 1.342 e Å^{-3}.

Single crystals of [TNF ⊂ **U_HAnt$_2$**] [$C_{55}H_{31}N_7O_7$] were grown by slow diffusion of cyclohexane into a chloroform solution. Crystals were placed in oil, and a single red crystal of dimensions 0.20 × 0.20 × 0.04 mm was mounted on a glass fiber and placed in a low-temperature N_2 stream. The cell was triclinic with a space group of *P*-1. Cell dimensions: $a = 9.3171$ Å, $b = 11.5016$ Å, $c = 20.4556$ Å, $\alpha = 80.867(5)°$, $\beta = 80.186(5)°$, $\gamma = 77.429(5)°$, $V = 2091.3(1)$, and $Z = 2$ (FW = 901.90 and $\rho = 1.43$ g/cm^{-3}). Reflections were collected $2.50° \leq \theta \leq 27.51°$ for a total of 9514 of which 3772 were unique, having $I > 3\sigma(I)$; number of parameters is 613. Final *R* factors were $R_1 = 0.071$ (based on observed data) and w$R_2 = 0.276$ (based on all data), GOF = 1.123, maximal residual electron density is 1.114 e Å^{-3}.

Single crystals of [phen ⊂ Zn^{II},**WAcr$_2$**] [$C_{55}H_{35}F_6N_7O_7S_2Zn$] were grown by slow diffusion of diethyl ether into an acetonitrile solution. Crystals were placed in oil, and a single orange crystal of dimensions 0.12 × 0.10 × 0.06 mm was mounted on a glass fiber and placed in a low-temperature N_2 stream. The cell was triclinic with a space group of *P*-1. Cell dimensions: $a = 13.0955(2)$ Å, $b = 13.1668(2)$ Å, $c = 15.9645(3)$ Å, $\alpha = 75.685(5)°$, $\beta = 84.946(5)°$, $\gamma = 64.653(5)°$, $V = 2409.96(7)$, and $Z = 2$ (FW = 1149.42 and $\rho = 1.58$ g/cm^{-3}). Reflections were collected $2.50° \leq \theta \leq 27.48°$ for a total of 10 798 of which 5337 were unique, having $I > 3\sigma(I)$; number of parameters is 703. Final *R* factors were $R_1 = 0.037$ (based on observed data) and w$R_2 = 0.167$ (based on all data), GOF = 1.015, maximal residual electron density is 0.268 e Å^{-3}.

Single crystals of [Zn^{II} ⊂ **W(CONHAnt)$_2$]**·2CF_3SO_3 [$C_{45}H_{29}N_5O_2$-Zn·2CF_3SO_3·2C_2H_3N] were grown by slow diffusion of diethyl ether into a mixture of acetonitrile and chloroform. Crystals were placed in oil, and a single orange crystal of dimensions 0.20 × 0.14 × 0.10 mm was mounted on a glass fiber and placed in a low-temperature N_2 stream. The cell was orthorhombic with a space group of *Pccn*. Cell dimensions: $a = 13.2654(2)$ Å, $b = 18.7260(3)$ Å, $c = 19.6692(4)$ Å, $\alpha = \beta = \gamma = 90°$, $V = 4886.0(1)$, and $Z = 4$ (FW = 1117.38 and $\rho = 1.52$ g/cm^{-3}). Reflections were collected $2.50° \leq \theta \leq 30.02°$ for a total of 7817 of which 4005 were unique, having $I > 3\sigma(I)$; number of parameters is 340. Final *R* factors were $R_1 = 0.033$ (based on observed data) and w$R_2 = 0.516$ (based on all data), GOF = 1.046, maximal residual electron density is 0.368 e Å^{-3}.

Acknowledgment. A.P. acknowledges the support of the French Ministère de l'Éducation et de la Recherche by a predoctoral fellowship and is indebted to Dr. T. Balaban for generously supplying the 2,3,6,7-tetrakis(dodecyloxy)anthracene (TDOA) used in this study. R.G.K. is grateful to the french government for a postdoctoral Chateaubriand fellowship.

Supporting Information Available: Crystallographic data (CIF). This material is available free of charge via the Internet at http://pubs.acs.org.

JA031915R